JOURNAL OF GEOPHYSICAL RESEARCH, VOL. 92, NO. C5, PAGES 5035–5044, MAY 15, 1987

The Upper Ocean Internal Wave Field: Influence of the Surface and Mixed Layer

MURRAY D. LEVINE

College of Oceanography, Oregon State University, Corvallis

A model is developed to calculate the upper ocean internal wave spectrum as modified by the surface boundary and mixed layer. The Garrett-Munk spectrum is assumed to describe the deep ocean wave field. The main effect of the surface and mixed layer is to align the vertical structure of the waves forming vertically standing waves locally; this contrasts with the assumption of random alignment in the Garrett-Munk model. Model spectra and coherences are calculated for idealized buoyancy frequency profiles and compared with the Garrett-Munk model. Measurements in the upper 200 m from the Mixed Layer Dynamics Experiment in the northeast Pacific in 1983 are also compared with the model results. The most striking success of the model is predicting the observed high coherence and 180° phase difference across the mixed layer of horizontal velocity.

1. INTRODUCTION

A kinematic description of oceanic internal waves is usually based on the hypothesis that the wave field is composed of a random sea of linear waves. For deep ocean internal waves the most widely known description is the one given by *Garrett and Munk* [1972, 1975] and summarized by *Munk* [1981] (hereinafter referred to as GM). The GM formulation assumes that the ocean has no top or bottom boundary and that the buoyancy frequency $N(z)$ varies slowly with depth compared with the fluctuations of the waves. This permits the vertical variation of wave amplitude and vertical wavelength to be scaled by $N(z)$ (WKB approximation). Other models, such as the Internal Wave Experiment (IWEX) model [*Müller et al.*, 1978], differ in detail but usually retain the basic tenets of the GM model. The GM model provides a standard with which to compare other models. In the upper ocean, say from the surface to 200 m, the GM model is expected to have limited application even discounting the possible effects of strong surface forcing or dissipation. This is because $N(z)$ is no longer a slowly varying function and because the surface acts as a boundary which can reflect waves. Despite these limitations, the GM spectrum has been compared with upper ocean measurements made by acoustic doppler profilers [*Pinkel*, 1984], moored current meters, and thermistor chains [*Käse and Siedler*, 1980; *Levine et al.*, 1983*a*, *b*], towed thermistor chains [*Bell*, 1976], and vertical conductivity, temperature, and depth profilers [*Pinkel*, 1975, 1981]. These comparisons indicate that while some aspects of the GM spectrum are consistent with the data, many are not. *Pinkel* [1981] has discussed and modeled some of the effects of the surface on the internal wave spectrum; this model is mostly concerned with the effects of a frequency dependent waveguide thickness but does not explicitly consider the effects of wave reflection at the surface.

The purpose of this paper is to develop a model that extends the GM formulation of the deep ocean internal wave field into the upper ocean by explicitly including the surface boundary and realistic upper ocean stratification. The deep ocean is still assumed to be composed of a collection of random waves with the amplitude distribution in frequency wave number space specified by GM. The modification of each upward-propagating wave is followed as the wave enters the upper ocean stratification and reflects off the surface; a standing wave in the vertical is formed locally. The statistical measures of the upper ocean wave field can be predicted by summing the contribution from all the waves. This procedure is analogous to that used to extend the GM model into the region near a turning point [*Desaubies*, 1973].

The spectral quantities calculated from the model can then be compared with upper ocean observations. The model provides a useful framework for interpreting internal wave measurements in the upper ocean in the same way as the GM spectrum does for the deep ocean. This comparison is a first step in studying the signature of other upper ocean processes, such as wind stress and solar heating, on internal wave observations.

The unique set of observations available from the Mixed Layer Dynamics Experiment (MILDEX) provides a good opportunity to compare model predictions with data. MILDEX took place in the northeast Pacific Ocean about 700 km west of Santa Barbara, California, during October–November 1983. Measurements were made in the upper 200 m of temperature and velocity from beneath a drifting buoy and temperature from a towed thermistor chain. From these data, frequency and horizontal wave number spectra and coherences were calculated and compared with the model.

The upper ocean spectral model is developed in section 2. Spectra and vertical coherences for idealized N profiles are then calculated from the model (section 3). In section 4, data from MILDEX are compared with the results of the model using the actual N profile. A summary and conclusion are presented in section 5.

2. MODEL

The first step in forming a statistical model of the upper ocean internal wave field is to determine the structure of a single wave component as it encounters the upper ocean. Since the model is linear, all of the components can then be added together using the amplitide distribution that will yield

Copyright 1987 by the American Geophysical Union.

Paper number 7C0227.
0148-0227/87/007C-0227$05.00

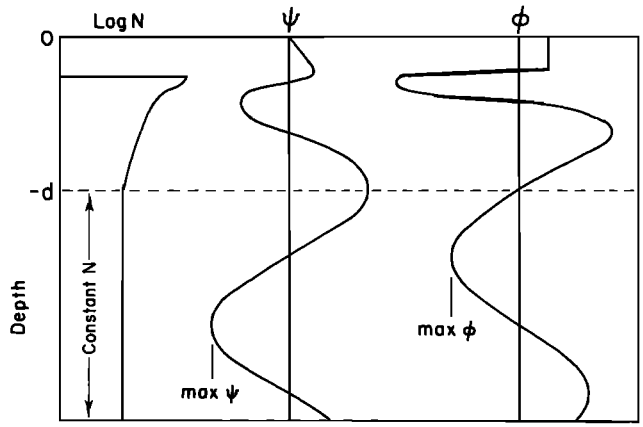

Fig. 1. Sample solution of ψ and ϕ for a typical N profile. Below $-d$, a constant N region is used to determine the maxima of ψ and ϕ needed for matching to the deep ocean GM spectra (equation (8)).

deep ocean statistics consistent with the GM spectrum.

Assume that the horizontal velocity and vertical displacement of a single, horizontally propagating plane wave can be written as

$$u(x, z, t) = \tilde{u}\phi(z) \exp [i(\alpha x - \omega t)] \quad (1a)$$

$$\zeta(x, z, t) = \tilde{\zeta}\psi(z) \exp [i(\alpha x - \omega t)] \quad (1b)$$

where $\phi = \alpha^{-1}(\partial\psi/\partial z)$, α is the horizontal wave number, ω is the frequency, and the real part of the right-hand side is implied.

The wave function $\psi(z)$ is determined by solving

$$\psi'' + \beta^2\psi = 0 \quad (2)$$

where

$$\beta^2(z) = \alpha^2 \frac{N^2(z) - \omega^2}{\omega^2 - f^2} \quad (3)$$

The surface is defined to be at $z = 0$, and $z = -d$ is the depth below which the internal waves statistics are assumed to behave as those specified by GM (Figure 1). Hence below $z = -d$ the wave function can be written as

$$\psi(z) = I \exp [-i\beta(z)z] + R \exp [i\beta(z)z] \quad (4)$$

where $\beta(z)$ is a slowly varying function of z, and I and R are the complex amplitudes of an incident (upward propagating energy) and reflected wave (downward propagating energy), respectively. Recall that for an internal wave the phase propagates upward (downward) while the energy propagates downward (upward). The z dependence is the same as used by GM and is a simplified form of the WKB approximation.

To solve (2) for an arbitrary $N(z)$ in the region above $z = -d$, boundary conditions at $z = 0$ and $-d$ are needed. With little error the surface is assumed to be rigid, $\psi(0) = 0$. Specifying the boundary at $z = -d$ is more subtle since the phase of the reflection is not known before solving the problem. Since no energy is lost upon reflection, $|I| = |R|$, but arg $I \neq$ arg R in general. Combining (4) and the derivative of (4), R can be eliminated, and the lower boundary condition can be expressed as a function of the incident wave amplitude only,

$$\psi' - i\beta\psi = -2i\beta I \exp [-i\beta(z)z] \quad \text{at } z = -d \quad (5)$$

Note that the assumption that β is slowly varying has been used in deriving (5). For a specified stratification the wave function $\psi(z)$ can be solved numerically for a given incident wave with amplitude I, wave number α, and frequency ω. There is only one solution of ψ; this is not an eigenvalue problem that results in an infinite number of modal solutions. This boundary value problem was solved using an efficient finite difference method due to *Lindzen and Kuo* [1969].

Spectral quantities can be calculated by summing the contribution from all the wave components. It is assumed that the collection of waves is horizontally isotropic, and there is no correlation among the components. The frequency cross spectra for horizontal velocity S_u and vertical displacement S_ζ between depths z_1 and z_2 can then be written [e.g., *Willebrand et al.*, 1977]

$$S_u(\omega, z_1, z_2) = \frac{(\omega^2 + f^2)(\omega^2 - f^2)^{1/2}}{2N(-d)} \cdot \sum_{n=1}^{n_{max}} \varepsilon_n(\omega)\phi_n(\omega, z_1)\phi_n(\omega, z_2) \quad (6a)$$

$$S_\zeta(\omega, z_1, z_2) = \frac{(\omega^2 - f^2)^{1/2}}{N(-d)} \sum_{n=1}^{n_{max}} \varepsilon_n(\omega)\psi_n(\omega, z_1)\psi_n(\omega, z_2) \quad (6b)$$

where f is the inertial frequency and $\varepsilon_n(\omega)$ is the spectral distribution function. The wave functions specify the vertical structure of a plane wave at frequency ω and horizontal wave number α_n,

$$\psi_n(\omega, z) = \psi(\alpha_n, \omega, z)$$

Equation (6) represents the spectra of a collection of n_{max} plane internal waves; for the results presented here, $n_{max} = 20$. The index n is often referred to as a "mode" number. However, in this application the vertical modes are not determined by solving the boundary value problem over the entire depth of the ocean. The spectral distribution function $\varepsilon_n(\omega)$ specifies the magnitude of each wave component at ω and α_n and is determined by matching the spectrum to the deep ocean GM spectrum at $z = -d$.

In the GM model, α is expressed as a function of n and ω (dispersion relation) using a modified WKB approximation:

$$\alpha_n(\omega) = \frac{n\pi}{b} \frac{(\omega^2 - f^2)^{1/2}}{N_0} \quad (7)$$

where b is the depth scale of $N(z)$ (1300 m), N_0 is the buoyancy scale (5.24×10^{-3} s^{-1} or 3 cph), and it is assumed that $\omega \ll N$. We choose the version of the GM formulation that partitions the energy into a discrete set of wave numbers ("modes") [*Munk*, 1981] rather than distributing it over a continuum [*Garrett and Munk*, 1972; 1975]. Note that α is not a function of z; the horizontal wave number does not change as a wave propagates through stratification that only varies in the vertical.

The most practical method to determine $\varepsilon_n(\omega)$, such that the spectrum matches the GM spectrum at $z = -d$, is to extend the numerical solution of ψ_n deeper than d into a region of constant $N = N(-d)$ (Figures 1). In this constant N region, ψ has a sinusoidal shape with vertical wave number β determined from (3).

The reason for solving ψ in this "artificial," constant N region is to determine the amplitude (maximum of $\psi_n(z)$) of

this wave component relative to the amplitude of the incident wave I. By equating the upper ocean spectrum (6) to the GM spectrum [*Munk*, 1981] the spectral distribution function is found

$$\varepsilon_n(\omega) = \frac{2}{\pi}\frac{H_n}{I^2}\frac{Eb^2N_0 f}{\omega^3 \max[\psi_n^2]} \tag{8}$$

where the parameter E is the nondimensional energy (6.3×10^{-5}) and the weighting function $H_n = \bar{H}^{-1}(j_*^2 + n^2)^{-1}$. The parameter j_* sets the wave number bandwidth of the spectral quantities and has a value of 3 in the GM model. The normalization constant $\bar{H}$ is chosen such that

$$\sum_n H_n = 1$$

In practice, I is set to an arbitrary constant, and (2) is solved numerically for $\psi_n(z)$ using (5) as the bottom boundary condition. The matching condition at $z = -d$ (equation (8)) then determines $\varepsilon_n(\omega)$ relative to this arbitrary constant such that the absolute value of the spectrum (equation (6)) equals the GM level.

To compare with data, two types of statistical quantities are investigated: moored and towed. This terminology follows the convention adopted by GM and refers to observations that are made from instruments which are fixed in space and instruments which profile horizontally. The moored spectrum of vertical displacement, MS_ζ, is a frequency autospectrum at a fixed location in space and is given by (6*b*)

$$MS_\zeta(\omega, z) = S_\zeta(\omega, z, z) \tag{9}$$

The moored vertical coherence of vertical displacement, MVC_ζ, is the coherence in frequency for a fixed vertical separation and is given by

$$MVC_\zeta(\omega; z_1, z_2) = \frac{S_\zeta(\omega, z_1, z_2)}{[S_\zeta(\omega, z_1, z_1)S_\zeta(\omega, z_2, z_2)]^{1/2}} \tag{10}$$

The towed spectrum of vertical displacement, TS_ζ, is the horizontal wave number spectrum at a fixed time and is given by

$$TS_\zeta(\alpha, z) = \frac{2}{\pi}\sum_n^{n_{max}}\int_{\omega_n}^{N(z)}\frac{S_\zeta(\omega, z, z)\,d\omega}{(\alpha_n^2 - \alpha^2)^{1/2}} \tag{11}$$

where

$$\omega_n^2 = f^2 + \left(\alpha\frac{bN_0}{n\pi}\right)^2 \tag{12}$$

TABLE 1. Summary of Model Cases

Case	Buoyancy Frequency	Spectral Composition
1a	constant, $N = N_0$	GM
1b	constant, $N = 3.2\ N_0$	GM
2a	step profile: $N = N_0$ below 50 m, $N = 0$ upper 50 m	GM
2b	step profile: $N = 3.2N_0$ below 50 m, $N = 0$ upper 50 m	GM
3a	MILDEX	GM
3b	MILDEX	GM but no contribution from $n = 1$, $\varepsilon_1 = 0$
3c	MILDEX	GM with frequency dependent waveguide, $bN_0 \rightarrow h(\omega)\,\bar{N}$

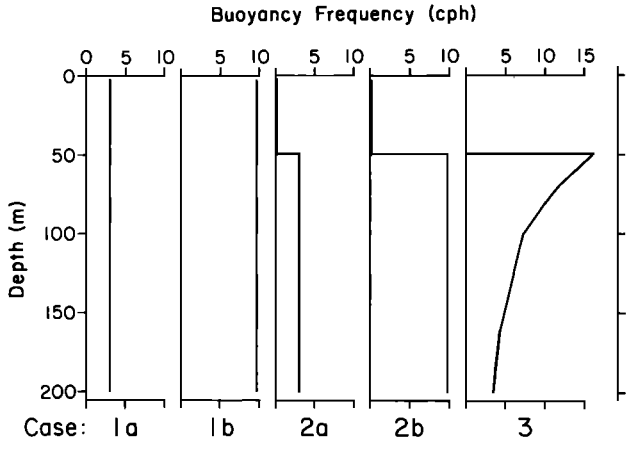

Fig. 2. Buoyancy frequency profiles used in calculating model spectra. Case 1 is constant N, case 2 is a step in N, and case 3 is the N profile from MILDEX.

The geometric factor in the denominator of the integrand accounts for the contribution to the one-dimensional wave number α from all wave numbers greater than α in a horizontally isotropic wave field. This integral was solved numerically by first transforming the integrand to remove the singularity in the denominator using the method of Iri, Moriguti, and Takasawa [*Atkinson*, 1978]. The towed vertical coherence of vertical displacement, TVC_ζ, is the coherence in horizontal wave number at a fixed vertical separation and is given by

$$TVC_\zeta(\alpha, z_1, z_2) = \frac{2/\pi}{[TS_\zeta(\alpha, z_1)TS_\zeta(\alpha, z_2)]^{1/2}} \cdot \sum_n^{n_{max}}\int_{\omega_n}^{N(z)}\frac{S_\zeta(\omega, z_1, z_2)\,d\omega}{(\alpha_n^2 - \alpha^2)^{1/2}} \tag{13}$$

The corresponding moored and towed spectral quantities for horizontal velocity have the exact same forms with the subscript ζ replaced by u.

3. Model Results—Idealized N Profiles

To illustrate the behavior of the model, two cases were run with idealized N profiles (Table 1): constant (case 1) and step profiles (case 2) (Figure 2). These cases were chosen to isolate the effects on the spectrum due to the presence of a surface boundary alone (case 1) and due to a mixed layer (case 2). The step profiles consist of a 50-m-deep mixed layer with $N = 0$ above a region of constant N. To examine the dependence on the absolute value of N, two values were used: $N = N_0$ (cases 1a and 2a) and $N = 3.2\ N_0$ (cases 1b and 2b). The value of f was chosen to be the same as at MILDEX (8.0×10^{-5} s^{-1}). In all the spectral calculations the model spectrum was matched to the GM spectrum at a depth of $d = 200$ m.

Constant N profile. A sample of the wave functions ψ and ϕ that determine the vertical structure of the spectra are shown in Figure 3. Since N is constant, the wave functions are purely sinusoidal. At higher N (case 1b) the vertical wave number is higher for a given α_n because of the dispersion relation (3).

The spectral shapes of the model in frequency (MS) and wave number (TS) nearly follow the GM prescription at all depths and therefore are not shown. The spectral levels as a function of depth are shown in Figure 4. According to the GM

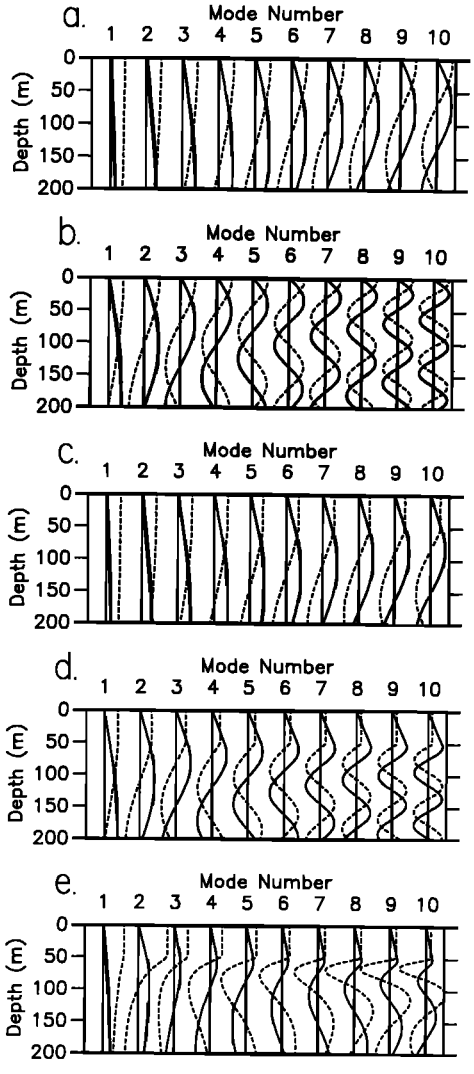

Fig. 3. Wave functions of vertical displacement ψ (solid lines) and horizontal velocity ϕ (dashed lines) as a function of depth for (*a*) case 1a, (*b*) case 1b, (*c*) case 2a, (*d*) case 2b, and (*e*) case 3.

model, the spectral level should be constant with depth in a constant N ocean. However, in the model there is some depth dependence of the spectra in an "adjustment region" near the surface. The vertical displacement spectra, MS_ζ and TS_ζ, go to zero at the surface as a result of the upper boundary condition; the wave functions ψ_n are zero at the surface. At higher N the vertical wave numbers are higher, and correspondingly, the adjustment region is smaller. The horizontal velocity spectra, MS_u and TS_u, are also affected by the surface boundary with an adjustment region that is approximately the same as for vertical displacement. At the surface the wave functions ϕ_n are at a maximum for all n, resulting in a spectral level that is 2–3 times greater near the surface than at depth.

Examples of the moored vertical coherences (MVC_u and MVC_ζ) at 1.4 cph and towed vertical coherences (TVC_u and TVC_ζ) at 10^{-4} cpm are contoured in Figures 5 and 6. The feature of the vertical coherences that differs most strikingly from the GM model is the presence of "negative" coherences. The sign of the coherence is used as shorthand notation to express the phase of the coherence: positive is in-phase (0°), negative is out-of-phase (180°). No other phases are possible in this simple model. The negative coherences are a result of the deterministic alignment of the wave functions caused by the reflection at the surface. Specifically, the reflection forces the maxima of ϕ and the zeros of ψ to occur at the surface. In the GM model there are no negative coherences because the alignment of the wave functions is random; all vertical coherences go to zero monotonically as the separation increases.

Other deviations from the GM model occur near the surface. In the GM model at constant N the contours would be straight, parallel lines at a 45° angle indicating that the coherence is a function of vertical separation only and not of absolute depth. The deviation from straight, parallel contours occurs primarily over the adjustment region. The presence of a reflecting surface has a relatively small effect on the near-surface coherences.

Step profile. For the step profile the assumption of a slowly varying $N(z)$, as used in the GM model, appears to be violated. Also, the GM spectrum is not defined within the mixed layer where $N = 0$. This model provides a method for extending the GM spectrum into the mixed layer, where vertically propagating internal waves cannot exist.

In the step profile the wave functions, and hence the spectra, differ from the constant N case primarily in the mixed layer. There is a turning point ($\omega = N(z)$) at the base of the mixed layer for waves of all frequency where the wave functions change behavior from oscillatory ($\omega < N(z)$) to exponential

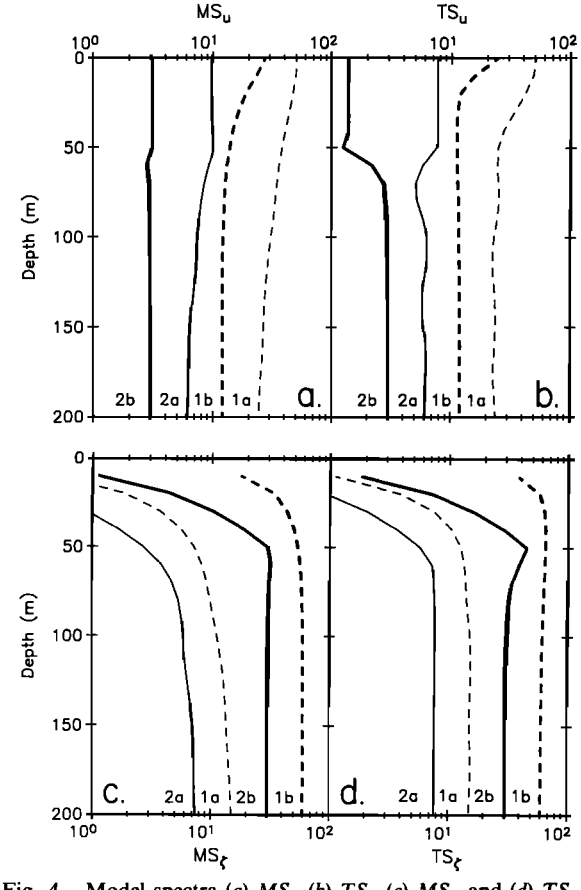

Fig. 4. Model spectra (*a*) MS_u, (*b*) TS_u, (*c*) MS_ζ, and (*d*) TS_ζ as a function of depth for case 1a (light dashed), case 1b (bold dashed), case 2a (light solid), and case 2b (bold solid). Absolute units of the spectra are arbitrary. Moored spectra (MS_u and MS_ζ) are evaluated at 1.4 cph; towed spectra (TS_u and TS_ζ) are evaluated at 10^{-4} cpm.

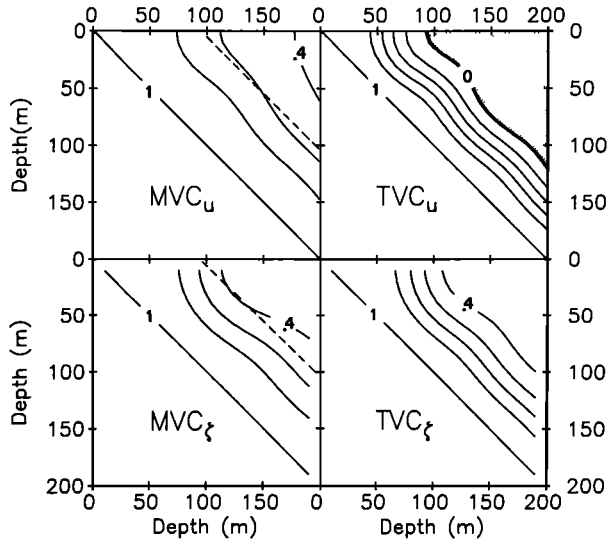

Fig. 5. Contour plot showing the model vertical coherences between any two depths for case 1a ($N = N_0$). The 1 contour is on the diagonal; the 0 contour is bold. Contour interval is 0.2; negative values are shaded. The 0.5-contour for the GM model is shown as a dashed line. The moored coherences (MVC) are evaluated at 1.4 cph; the towed coherences (TVC) are evaluated at 10^{-4} cpm.

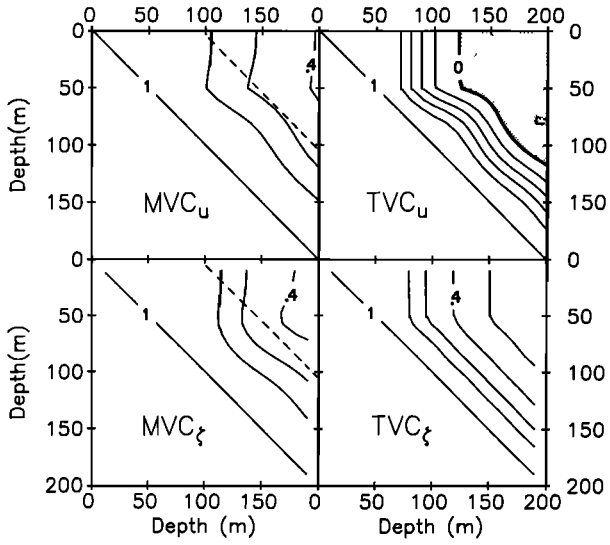

Fig. 7. Contour plot showing the model vertical coherences between any two depths for case 2a (Step of N_0). The 1 contour is on the diagonal; the 0 contour is bold. Contour interval is 0.2; negative values are shaded. The 0.5 contour for the GM model is shown as a dashed line. The moored coherences (MVC) are evaluated at 1.4 cph; the towed coherences (TVC) are evaluated at 10^{-4} cpm.

($\omega > N(z)$). The wave functions ϕ_n are nearly constant, and ψ_n are nearly linear in the upper 50 m (Figure 3). At large vertical wavelengths (low modes) the wave functions are similar to the constant N cases; the effect of the relatively small, mixed layer is slight. For waves with a vertical wavelength comparable or smaller than the mixed layer there are zero crossings in ψ and maxima in ϕ near 50 m depth (Figure 3).

Below 50 m the spectra are similar to the constant N spectra (Figure 4). In the mixed layer, vertical displacement spectra (MS_ζ and TS_ζ) decrease to zero at the surface as in the constant N case. The difference is that the decrease occurs in the mixed layer whether the adjustment region is larger or smaller than the mixed layer depth. The velocity spectra (MS_u and TS_u) are nearly uniform in the mixed layer because the ϕ_n are nearly uniform. However, the spectral level in the mixed layer is slightly higher than the deep spectrum at low N (case 2a) and becomes lower at high N (case 2b).

The main differences in the coherences of the step profile compared with the constant N case also occur in the mixed layer (Figures 7 and 8). At a fixed vertical separation the coherence within the mixed layer is higher than it is for the same separation in the constant N case. The differences are

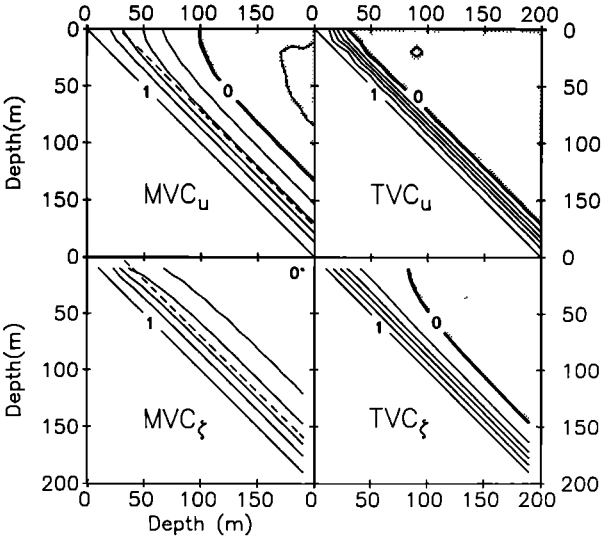

Fig. 6. Contour plot showing the model vertical coherences between any two depths for case 1b ($N = 3.2\ N_0$). The 1 contour is on the diagonal; the 0 contour is bold. Contour interval is 0.2; negative values are shaded. The 0.5 contour for the GM model is shown as a dashed line. The moored coherences (MVC) are evaluated at 1.4 cph; the towed coherences (TVC) are evaluated at 10^{-4} cpm.

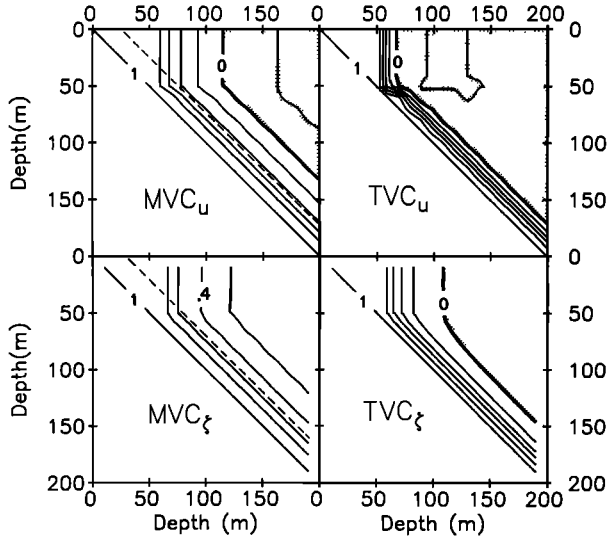

Fig. 8. Contour plot showing the model vertical coherences between any two depths for case 2b (Step of 3.2 N_0). The 1 contour is on the diagonal; the 0 contour is bold. Contour interval is 0.2; negative values are shaded. The 0.5 contour for the GM model is shown as a dashed line. The moored coherences (MVC) are evaluated at 1.4 cph; the towed coherences (TVC) are evaluated at 10^{-4} cpm.

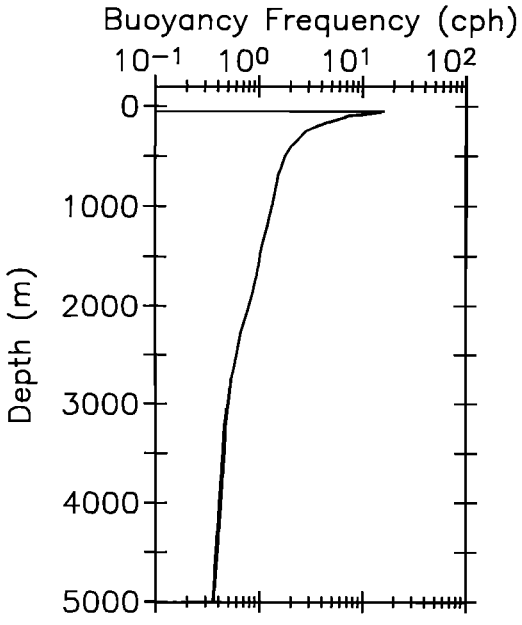

Fig. 9. Buoyancy frequency profile for MILDEX.

due to the absence of zero crossings in the wave functions in the mixed layer. Below the mixed layer the coherence structure is nearly the same as the corresponding constant N case.

4. MILDEX: Model and Observations

The statistical model developed in section 2 is compared with observations made during the Mixed Layer Dynamics Experiment (MILDEX). Three cases of the model are run with the N profile observed during MILDEX. The cases differ in the details of the spectral distribution function (Table 1). One of the cases (3a) uses the same $\varepsilon_n(\omega)$ as in section 2; the other two cases (3b and 3c) are small modifications of the weighting used in the GM model. Observed spectra and coherences are then compared with the model results.

Model. The only data needed to calculate the model spectra for the MILDEX site is the buoyancy frequency profile. A composite N profile of the entire water column was created from several sources (Figure 9). The stratification in the upper 75 m is taken from a typical single profile observed by the Rapid Sampling Vertical Profiler [*Newberger et al.*, 1984]. A single realization is more representative than an average profile where the sharp thermocline is smeared out due to the averaging of many profiles each of which has been displaced vertically by internal waves. The profile was completed using observations to 300 m made aboard Research Platform Flip (R. Pinkel, personal communication, 1986) and profiles to 800 m made aboard the R/V *Acania* (T. Stanton, personal communication, 1986). Deeper values of N were estimated from historical data averaged in 1° × 1° squares by *Levitus* [1982]. An enlarged view of the N profile in the upper 200 m is shown in Figure 2.

First, model spectra and coherences were calculated (case 3a) using the same GM parameters E, j_*, b, and N_0 and the same spectral distribution function, $\varepsilon_n(\omega)$, as in section 2. For this case the model spectra are qualitatively similar to the results from the idealized step profile (case 2). In case 3a, $N(z)$ decreases below 50 m, while in case 2, N is constant below the mixed layer.

Two other cases were also run with the MILDEX N profile but using modified spectral distribution functions (Table 1). In case 3b the contribution from mode 1 is eliminated. This is accomplished by setting $H_1 = 0$ and changing the normalization constant $\bar{H}$; H_n for $n > 1$ is unchanged (equation (8)). Case 3b demonstrates the effect of increasing the horizontal wave number that has the most energy. As will be seen, the motivation for eliminating mode 1 is to improve dramatically the agreement between model and observed coherences. It may seem ad hoc to eliminate mode 1; however, the observational evidence that indicates the dominance of mode 1 in the GM model is not conclusive. The results from IWEX [*Müller et al.*, 1978] show that mode 1 may be relatively less energetic than the GM prescription. Other observations have also shown that the model fit is improved using a higher value of j_* [e.g., *Levine et al.*, 1986]; the effect of higher j_* is to reduce the magnitude of mode 1 relative to the other modes. While totally eliminating mode 1 is extreme, this case serves as an indication of the effect on the spectrum for a decrease in the relative magnitude of mode 1.

In case 3c the GM form of the dispersion relation (7) is modified to model more realistically a variable N profile. In the GM model the vertical scale of the wave is a constant, b. A more accurate parameterization allows for a variation in the vertical scale of the waveguide as a function of frequency, $h(\omega)$. For MILDEX an estimate of $h(\omega)$ is taken to be the depth range below the mixed layer where $\omega < N(z)$. To be consistent, a modification of the stratification scale N_0 in (7) is also made. The scale N_0 is replaced by the average buoyancy frequency $\bar{N}$ over the waveguide $h(\omega)$. At low frequency, $h(\omega)$ approaches the depth of the ocean and $\bar{N}$ is a minimum. As frequency increases, $h(\omega)$ becomes smaller while $\bar{N}$ increases; the net effect for MILDEX is a decrease of the produce $h(\omega)\,\bar{N}$ as frequency increases. The consequence of replacing $N_0 b$ by $\bar{N}h(\omega)$ in (7) is to modify the horizontal wave number as a function of n and ω. At high frequency, α has a larger value

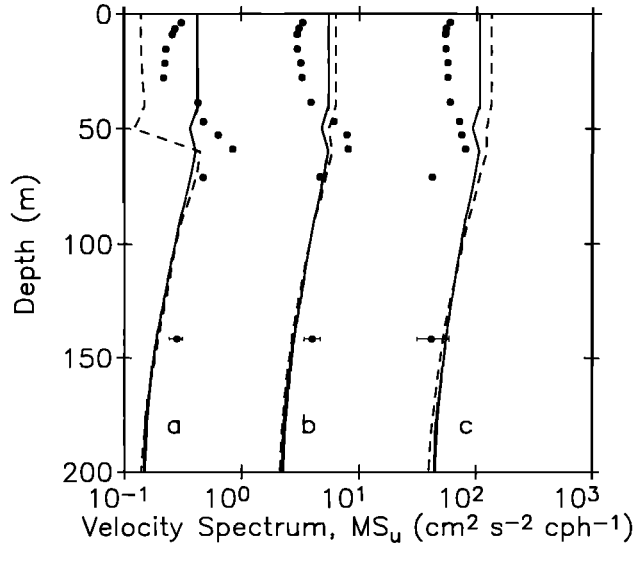

Fig. 10. Moored velocity spectra, 1/2 ($MS_u + MS_v$), as a function of depth for frequency bands (*a*) 1.5–3.0 cph, (*b*) 0.375–0.75 cph, and (*c*) 0.0937–0.1875 cph. Data are shown as solid circles; model results are plotted as solid lines (case 3a) and dashed lines (case 3c). The 95% confidence limits are indicated on the deepest values.

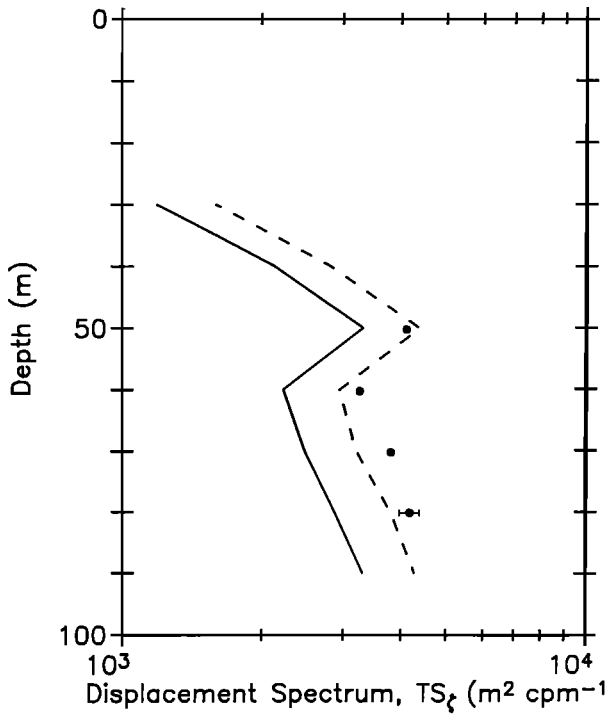

Fig. 11. Towed spectrum of vertical displacement as a function of depth for the wave number band 10^{-4}–10^{-3} cpm. Data are shown as solid circles; model results are plotted as a solid line (case 3a) and a dashed line (case 3b). The 95% confidence limits are indicated on the deepest value.

than in case 3a at the same ω and n. As a result, the spectral quantities for case 3c are a much stronger function of frequency, especially at high frequency.

In all of these calculations no quantities have been calculated at frequencies above $N(-d) = 3.5$ cph. This is because there is no energy above local N in the GM model; above N, freely propagating internal waves cannot exist. It is possible to extend the analysis by using a different method at high frequency to set the spectral level, but this would complicate the straightforward objective of this paper.

Observations compared with model. The model is compared with MILDEX observations from a drifter and a towed thermistor chain. The drifter consisted of a free-floating toroid buoy that was instrumented below with a string of 15 Vector-Measuring Current Meters from 3 to 141 m and 4 Aanderaa thermistor chains from 70 to 800 m [*Levine et al.* 1984]. The deployment was near 33°51′ N, 126°42′ W; recovery occurred 19 days later about 80 km northeast. The thermistor chain was towed in the MILDEX area from the R/V *Wecoma* a total of nearly 2000 km [*Baumann et al.*, 1985]. Twenty-eight temperature sensors spanned the surface to 95 m depth.

First, the autospectra of the data and model are compared. The depth dependence of the observed autospectra MS_u and TS_ζ are shown with the model results in Figures 10 and 11. The observed and modeled MS_u are plotted together as a function of depth for several frequency bands (Figure 10). Below the mixed layer there is not much to distinguish among the model cases 3a, 3b, and 3c. The absolute level and the depth dependence of the data reasonably follows the model; however, the agreement is worse at low frequency. Within the mixed layer the spectral levels vary more in the vertical than indicated by the internal wave model. This is not too surprising as there are many other sources of variability in the mixed layer that are clearly not due to free, linear internal waves. While the model spectral level does not agree perfectly with the observations, it is certainly better than the GM model, which is not defined in the mixed layer where N goes to zero. The observed spectral level in the mixed layer decreases relative to 70 m as frequency increases. Model case 3c with the frequency dependent waveguide also exhibits this same general behavior.

The depth dependence of the TS_ζ as observed by the towed thermistor chain in the wave number band from 10^{-4} to 10^{-3} cpm is shown with the model results in Figure 11. As with MS_u, the model cases 3a, 3b, and 3c are similar. The data follow the model remarkably well indicating a slight maximum near 50 m. The absolute values are best fit by case 3c although there is less than a factor of 1.5 separating the cases. The GM model has no maximum but increases monotonically with depth following $1/N$ scaling.

Although data are not available to estimate all possible autospectra, it is interesting to compare the depth dependence of the modeled MS_ζ, MS_u, TS_ζ, and TS_u (Figure 12). As the distance below the mixed layer increases, the spectra more nearly follow the N scaling expected from the WKB approximation, that is, velocity spectra scale as $N(z)$ and vertical displacement spectra scale as $1/N(z)$. In the mixed layer, where N scaling is obviously not valid, the u spectra are nearly constant with depth, and the ζ spectra decrease uniformly to zero at the surface, similar to the idealized step profile (case 2b).

A comparison of the frequency and wave number dependence of the observed and modeled autospectra MS_u, MS_ζ, and TS_ζ are examined in Figures 13, 14, and 15. Frequency spectra MS_u from 15 and 141 m are plotted with the model

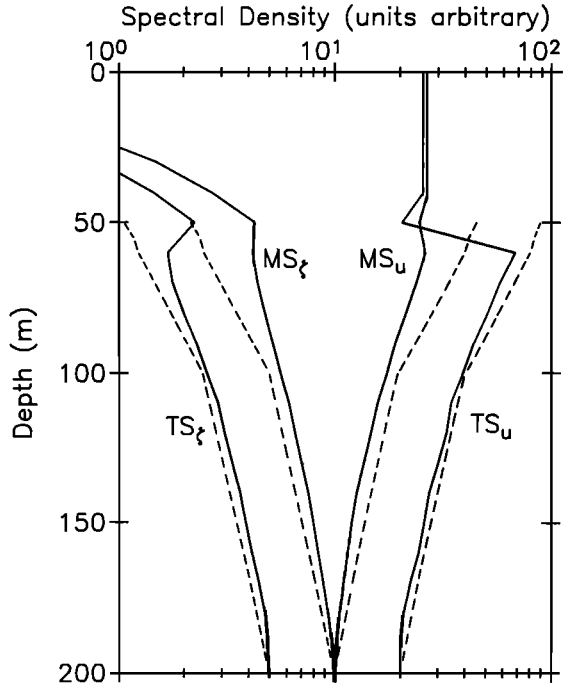

Fig. 12. Model spectra as a function of depth for case 3a. Absolute units of the spectra are arbitrary. Moored spectra (MS_u and MS_ζ) are evaluated at 1.4 cph; towed spectra (TS_u and TS_ζ) are evaluated at 10^{-4} cpm. Buoyancy frequency scaling (WKB approximation) is shown as dashed lines.

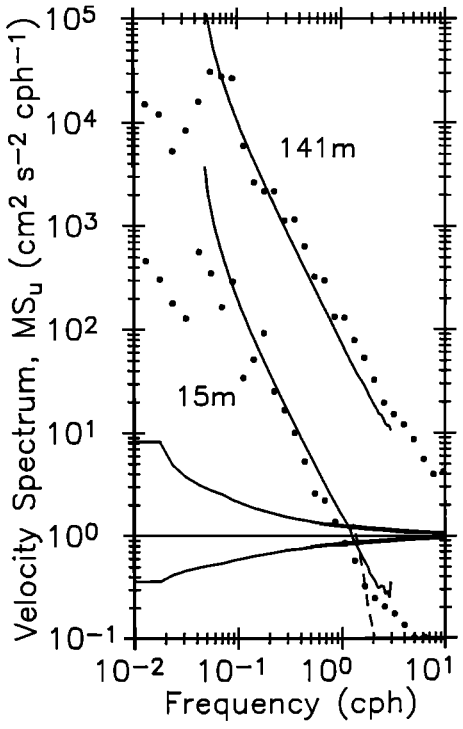

Fig. 13. Moored velocity spectra, $\frac{1}{2}(MS_u + MS_v)$, as a function of frequency at 15 (no offset) and 141 m (offset by factor of 100). Data are shown as solid circles. Model results are plotted as solid lines (case 3a). The portion of model case 3c that differs significantly from case 3a is shown as a dashed line. The 95% confidence limits are indicated.

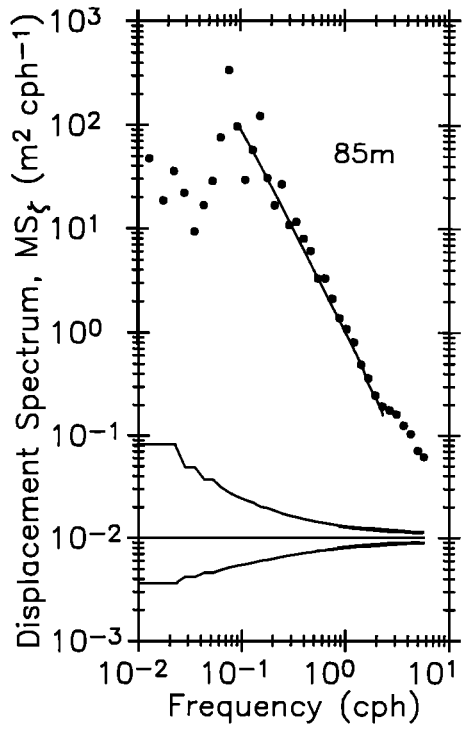

Fig. 14. Moored vertical displacement spectrum, MS_ζ, at 85 m. Data are shown as solid circles; model results (case 3a) are plotted as a solid line. The 95% confidence limits are indicated.

spectra in Figure 13. Again, only case 3a is plotted as the model results for the other cases are nearly the same. The greatest difference among the cases occurs in case 3c at high frequency where there is a sharp decrease in the spectrum in the mixed layer. The model spectral shape represents the data reasonably well; however, there are differences in the levels. At 15 m in the mixed layer the model is a bit higher than the observations; the GM spectrum is not defined where $N = 0$. At 141 m the model is lower than the data. This difference is not due to a difference between the model and GM spectrum since they are virtually identical at this depth.

A good estimate of the vertical displacement spectrum MS_ζ is available only at 85 m from the moored thermistor chain (Figure 14). As with the MS_u, the differences among the cases and the GM model are slight; however, the agreement with the observations is good.

The wave number dependence of the observed TS_ζ at 50 m is compared with the model in Figure 15. The agreement between the model and data is good, especially in the midband of wave numbers. The model level is higher than the GM spectrum at low wave numbers and fits the data better. The model results become less valid at high wave numbers since no contributions from frequencies beyond 3 cph were used.

In contrast to the autospectra the model coherences vary substantially among cases 3a, 3b, and 3c. A detailed comparison of the model MVC_u with three observed coherences is presented in Figure 16. In the GM model the MVC_u is not a function of the absolute depth but only of the vertical separation; the larger the separation, the smaller the coherence, with the phase always zero. Clearly, the data to not follow this behavior. The largest separation of 126 m (15–141 m) has a 180° phase difference with a higher coherence in general than the smaller separations of 55 m (15–70 m) and 71 m (70–141 m). Case 3a reproduces the observed phase structure; however, the coherence between 15 and 141 m is much smaller than observed. When mode 1 is eliminated (case 3b), the coherence increases dramatically. This is because the most energetic "modes" now have a single zero crossing between 15 and 141 m (Figure 3). The agreement of the model with the other

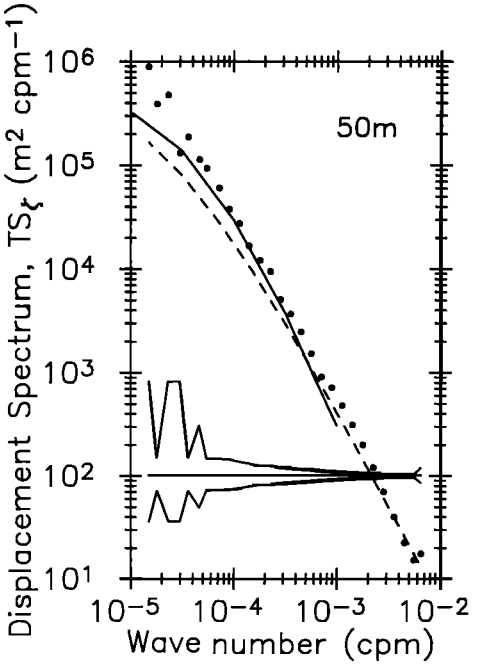

Fig. 15. Towed spectrum of vertical displacement, TS_ζ, at 50 m. Data are shown as solid circles; model results (case 3a) are plotted as a solid line. The GM model is plotted as a dashed line.

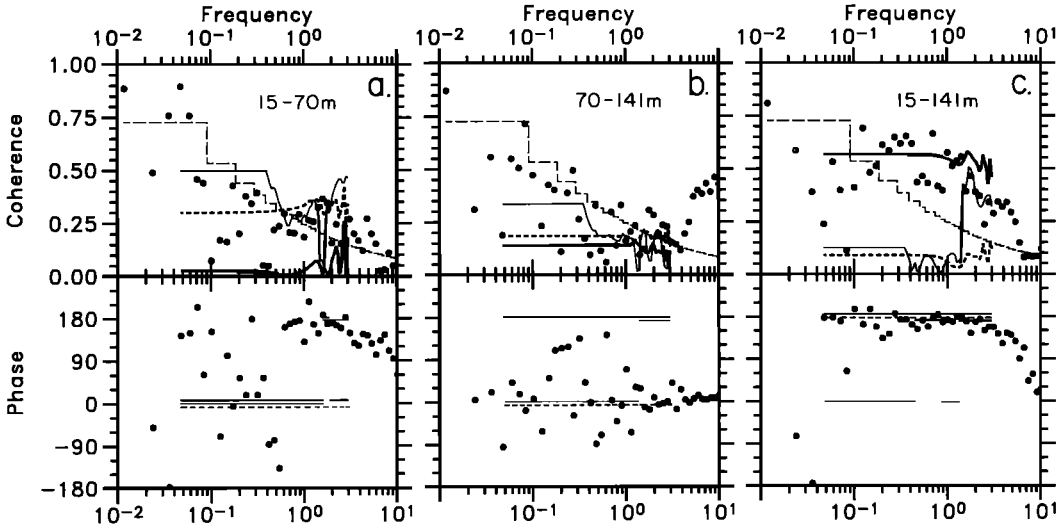

Fig. 16. Moored vertical coherence of velocity, MVC_u, between (*a*) 15 and 70 m, (*b*) 70 and 141 m, and (*c*) 15 and 141 m. Data are plotted as solid circles. Model coherences for case 3a (bold dashed), case 3b (bold solid), and case 3c (light solid) are also shown. Data above the light dashed line are significantly nonzero at the 90% confidence limit.

coherences is not as good; however, it does show significantly lower coherence at a smaller separation. Case 3c with the variable waveguide scaling is similar to case 3a at low frequency; hence the agreement with the observations is not very good. However, at high frequency in the 1.5- to 3-cph band the model coherence has a peak with a 180° phase difference between 15 and 141 m which agrees well with the data, although no better than case 3b. Case 3c also predicts a peak with a 180° phase difference between 15 and 70 m; while this does not quite agree with the observations, a similar feature does occur at a slightly lower-frequency band.

5. Summary and Conclusions

The main purpose of this paper is to develop a formalism to calculate the effect of the surface boundary and the mixed layer on the spectral quantities of the internal wave field. It is assumed that the deep ocean wave field follows the Garrett-Munk description. The alteration of the wave field in the upper ocean is assumed to be due to the vertical variation of $N(z)$ and the presence of a surface boundary. The structure of each wave component is tracked as it propagates into the upper ocean from the GM ocean below. All the wave components are then added together to produce estimates of spectral quantities in the upper ocean.

The results of the model are useful in interpreting upper ocean measurements by indicating the modifications in spectra and coherences that can be attributed directly to the kinematic distortion of the deep ocean internal wave field. In order to study other aspects of the upper ocean wave field it is first necessary to understand the passive effect of the surface and the upper ocean stratification. This is especially important when comparing observations made in regions with radically different N profiles.

The spectral features of the upper ocean model that differ from the GM spectrum are due to the nonrandom alignment in depth of the vertical wave functions. In the GM model the phase relationship among the vertical "modes" is assumed to be random. This may be a resonable assumption in the deep ocean. However, near a reflecting boundary, such as the ocean surface or the base of the mixed layer, a vertically standing wave is formed. The underlying premise here is that there is a strong tendency in the wave field toward random phases among the modes but that the phase relationships become more deterministic in the vicinity of a reflecting surface.

The best way to apply this model to a data set is to solve it with the appropriate N profile. However, a qualitative indication of the effect on the spectra can be obtained by examining the results from two idealized N profiles (Table 1): constant (case 1) and a step profile with $N = 0$ in the upper 50 m mixed layer (case 2) (Figure 2). The effect of the surface boundary alone can be examined in the constant N ocean (case 1); variations of the spectral quantities in the vertical are caused by the particular alignment of all wave components and not fluctuations in $N(z)$. Specific features that differ from GM are as follows: (1) the deviations from the GM spectrum and coherences occur near the surface in an adjustment region, which is smaller at higher N, (2) at the surface, vertical displacement spectra (MS_ζ and TS_ζ) go to zero, and velocity spectra (MS_u and TS_u) are a maximum (Figure 4), (3) "negative" coherences are possible, and (4) vertical coherences of ζ (MVC_ζ and TVC_ζ) decrease toward the surface in the adjustment region while those of u (MVC_u and TVC_u) increase; very near the surface all coherences increase (Figures 5 and 6).

The addition of a mixed layer (case 2), whose depth is small relative to the horizontal wavelength of the wave, causes the ϕ wave functions to be nearly uniform and the ψ wave functions to be nearly linear in the mixed layer (Figure 3). Below the mixed layer the vertical wavelength of each component is a function only of N (equation (7)), and hence the vertical wavelengths in cases 1a and 1b are the same as in cases 2a and 2b, respectively. At lower wave numbers (lower modes) the mode shapes for the step profile are nearly the same as for the constant N case (Figure 3). However, at higher wave number (higher modes) the phase of the vertical structure for the step profile is significantly shifted relative to the constant N case; the depth of the shallowest zero crossing has been shifted deeper in cases 2a and 2b compared with cases 1a and 1b for the same mode. The major differences in the spectral quantities between the step profile cases (cases 2a and 2b) and the constant N cases (cases 1a and 1b) occur in the mixed layer

and can be summarized as follows: (1) in the mixed layer the spectra of velocity (MS_u and TS_u) are nearly uniform, and the spectral level is relatively higher for a lower value of deep N (Figure 4), (2) Spectra of vertical displacement (MS_ζ and TS_ζ) decrease in the mixed layer to zero at the surface (Figure 4), and (3) All vertical coherences are higher than the corresponding constant N case when at least one of the two depths are in the mixed layer (Figures 7 and 8).

To apply the model to a realistic situation, the spectral quantities were calculated for the N profile observed during the Mixed Layer Dynamics Experiment (MILDEX) (Figures 2 and 9). The farther below the mixed layer, the more closely the modeled autospectra (TS_ζ, MS_ζ, TS_u, MS_u) follow the N scaling of the WKB approximation (Figure 12). The deviation from N scaling is greatest just below the mixed layer and, of course, in the mixed layer itself where N scaling is not possible. It may seem somewhat surprising that the WKB approximation works as well as it does since there is significant vertical variation in N compared with the wave functions, especially at the energetic, low modes. This result implies that significant deviations from N scaling of observed spectra are due to real differences in the GM model and not just kinematic effects of the upper boundary.

Some features of the depth dependence of the spectral model can be found in the observed spectra, TS_ζ and MS_u. Estimates of TS_ζ at several depths follows the model remarkably well (Figure 11); the slight maximum at 50 m does not occur in the N-scaled GM model. The comparison of the observed and modeled MS_u is perhaps not as convincing; however, some features of the model do occur in the data (Figure 10). For example, the observed spectrum in the mixed layer tends to be uniform with depth. Some of the measured variability may be due to the variation of the structure of the mixed layer over the duration of the experiment; the increase near the surface is probably due to direct atmospheric forcing. At higher frequency the data show lower spectral levels in the mixed layer relative to 70 m. This behavior is mimicked by model case 3c with the frequency dependent waveguide.

The frequency dependence of the modeled MS_u and MS_ζ are compared with observations in Figures 13 and 14. The model provides a reasonable fit to the observed MS_u at 15 m, certainly better than the GM spectrum which is undefined in the mixed layer.

The greatest success of the model is in explaining the high vertical coherence with a 180° phase between 15 and 141 m (Figure 16). In the GM model the coherence decreases monotonically as a function of vertical separation with zero phase difference. Case 3a predicts the 180° difference, but the coherence is much too small. While a systematic investigation of the effect of modifying the GM spectrum is beyond the scope of this paper, some simple alterations to the GM spectrum were made in cases 3b and 3c. When mode 1 is eliminated (case 3b), the agreement between data and model is much improved; this case also follows the data by predicting lower coherence between 15 and 70 m and between 70 and 141 m than between 15 and 141 m. At high frequency the frequency dependent waveguide (case 3c) provides a reasonable fit to the data. This is consistent with the improved agreement in case 3c of the velocity spectral level MS_u in the mixed layer (Figure 10). Overall, case 3b with no contribution from mode 1 fit the data better than 3a. This suggests that the lowest horizontal wave number according to the GM scaling is not the most energetic at MILDEX. There is also evidence of a frequency dependent vertical waveguide at high frequency (case 3c).

Acknowledgments. I thank James Richman for orchestrating the Drifter experiment and providing me with the current meter data, and Roland deSzoeke, Lloyd Regier, and Russ Davis for their role in planning, preparing, and deploying the Drifter. I also thank Clayton Paulson for allowing me to use the towed thermistor chain data, and Robert Pinkel and Tim Stanton for supplying the N profile data. The efforts of Eric Beals in carrying out the numerical analysis and Steve Gard in preparing the final figures are greatly appreciated. Discussions with Phyllis Stabeno and Teresa Chereskin were most useful. The support by the Office of Naval Research under contract N00014-84-C-0218 is gratefully acknowledged.

REFERENCES

Atkinson, K. E., *An Introduction to Numerical Analysis*, p. 269, John Wiley, New York, 1978.

Baumann, R. J., L. M. deWitt, C. A. Paulson, J. V. Paduan, and J. D. Wagner, Towed thermistor chain observations during MILDEX, *Ref. 85-12*, 135 pp., Coll. of Oceanogr., Oreg. State Univ., Corvallis, Oreg., 1985.

Bell, T. H., The structure of internal wave spectra as determined from towed thermistor chain measurements, *J. Geophys. Res., 81*, 3709–3714, 1976.

Desaubies, Y. J. F., Internal waves near the turning point, *Geophys. Fluid Mech., 5*, 143–154, 1973.

Garrett, C. J. R., and W. H. Munk, Space-time scales of internal waves, *Geophys. Fluid Dyn., 2*, 225–264, 1972.

Garrett, C. J. R., and W. H. Munk, Space-time scales of internal waves: A progress report, *J. Geophys. Res., 80*, 291–297, 1975.

Käse, R. H., and G. Siedler, Internal wave kinematics in the upper tropical Atlantic, *Deep Sea Res., 26*, suppl., 161–189, 1980.

Levine, M. D., R. A. deSzoeke, and P. P. Niiler, Internal waves in the upper ocean during MILE, *J. Phys. Oceanogr., 13*, 240–257, 1983*a*.

Levine, M. D., C. A. Paulson, M. G. Briscoe, R. A. Weller, and H. Peters, Internal waves in JASIN, *Philos. Trans. R. Soc. London, Ser. A, 308*, 389–405, 1983*b*.

Levine, M. D., S. R. Gard, and J. Simpkins, Thermistor chain observations during MILDEX, *Ref. 84-9*, 159 pp., Coll. of Oceanogr., Oreg. State Univ., Corvallis, Oreg., 1984.

Levine, M. D., J. D. Irish, T. E. Ewart, and S. A. Reynolds, Simultaneous spatial and temporal measurements of the internal wave field during MATE, *J. Geophys. Res., 91*, 9709–9719, 1986.

Levitus, S., *Climatological Atlas of the World Ocean*, NOAA Prof. Pap. 13, U.S. Department of Commerce, Washington, D. C., 1982.

Lindzen, R. S., and H.-L. Kuo, A reliable method for the numerical integration of a large class of ordinary and partial differential equations, *Mon. Weather Rev., 97*, 732–734, 1969.

Müller, P., D. J. Olbers, and J. Willebrand, The IWEX spetrum, *J. Geophys. Res., 83*, 479–500, 1978.

Munk, W. H., Internal waves and small-scale processes, in *Evolution of Physical Oceanography*, edited by B. A. Warren and C. Wunsch, pp. 264–291, MIT Press, Cambridge, Mass., 1981.

Newberger, P. A., H. H. Dannelongue, and D. R. Caldwell, The rapid sampling vertical profiler, MILDEX, October–November 1983, *Ref. 84-4*, 123 pp., Coll. of Oceanogr., Oreg. State Univ., Corvallis, Oreg., 1984.

Pinkel, R., Upper ocean internal wave observations from Flip, *J. Geophys. Res., 80*, 3892–3910, 1975.

Pinkel, R., Observations of the near-surface internal wavefield, *J. Phys. Oceangr., 11*, 1248–1257, 1981.

Pinkel, R., Doppler sonar observations of internal waves: The wavenumber-frequency spectrum, *J. Phys. Oceanogr., 14*, 1249–1270, 1984.

Willebrand, J., P. Müller, and D. J. Olbers, Inverse analysis of the trimoored internal wave experiment (IWEX), *Number 20a*, Ber. aus dem Inst. für Meereskunde an der Christ.-Albrechts-Univ., Kiel, Federal Republic of Germany, 1977.

M. D. Levine, College of Oceanography, Oregon State University, Corvallis, OR 97331.

(Received August 18, 1986;
accepted January 14, 1987.)